Published in final edited form as:
J Mol Biol. 2009 February 27; 386(3): 773–788. doi:10.1016/j.jmb.2008.12.073.

Effect of Mg^{2+} and Na^{+} on the Nucleic Acid Chaperone Activity of HIV-1 Nucleocapsid Protein: Implications for Reverse Transcription

Vo My-Nuong[1,†], **George Barany**[1], **Ioulia Rouzina**[1,2,*], and **Karin Musier-Forsyth**[3,*]

1*Department of Chemistry and Institute for Molecular Virology, University of Minnesota, Minneapolis, MN 55455*

2*Department of Biochemistry, Molecular Biology and Biophysics, University of Minnesota, Minneapolis, MN 55455*

3*Departments of Chemistry and Biochemistry, The Ohio State University, Columbus, OH 43210*

Summary

The human immunodeficiency virus type 1 (HIV-1) nucleocapsid protein (NC) is an essential protein for retroviral replication. Among its numerous functions, NC is a nucleic acid (NA) chaperone protein that catalyzes NA rearrangements leading to the formation of thermodynamically more stable conformations. *In vitro*, NC chaperone activity is typically assayed under conditions of low or no Mg^{2+}, even though reverse transcription requires the presence of divalent cations. Here, the chaperone activity of HIV-1 NC was studied as a function of varying Na^{+} and Mg^{2+} concentrations by investigating the annealing of complementary DNA and RNA hairpins derived from the *trans*-activation response domain of the HIV genome. This reaction mimics the annealing step of the minus-strand transfer process in reverse transcription. Gel-shift annealing and sedimentation assays were used to monitor the annealing kinetics and aggregation activity of NC, respectively. In the absence of protein, a limited ability of Na^{+} and Mg^{2+} cations to facilitate hairpin annealing was observed, whereas NC stimulated the annealing 10^{3}- to 10^{5}-fold. The major effect of either NC or the cations is on the rate of bimolecular association of the hairpins. This effect is especially strong under conditions wherein NC induces NA aggregation. Titration with NC and NC/Mg^{2+} competition studies showed that the annealing kinetics depends only on the level of NA saturation with NC. NC competes with Mg^{2+} or Na^{+} for sequence non-specific NA binding similar to a simple trivalent cation. Upon saturation, NC induces attraction between NA molecules corresponding to ~0.3 kcal/mol/nucleotide, in agreement with an electrostatic mechanism of NC-induced NA aggregation. These data provide insights into the variable effects of NC's chaperone activity observed during *in vitro* studies of divalent metal-dependent reverse transcription reactions, and suggest the feasibility of NC-facilitated proviral DNA synthesis within the mature capsid core.

*Corresponding authors: Email addresses of the corresponding authors: musier@chemistry.ohio-state.edu; rouzi002@umn.edu.
†Present address: The Scripps Research Institute, 10550 North Torrey Pines Road, La Jolla, CA 92037

Keywords

nucleic acid chaperone activity; HIV-1 nucleocapsid protein; nucleic acid aggregation; multivalent cations; electrostatics of nucleic acids

Introduction

Human immunodeficiency virus type 1 (HIV-1) nucleocapsid protein (NC) is a highly cationic 55-amino acid protein derived upon proteolysis of the Gag and Gag-Pol polyprotein precursors [1-3]. Like most other retroviral NC proteins, HIV-1 NC, or the NC domain of Gag, is known to play a role in packaging viral RNA [4; 5] or non-viral RNA [6-8], virus assembly [9-12], viral RNA dimerization [13; 14] and maturation [15; 16], tRNA primer annealing to the viral RNA template [14; 17-20], reverse transcription [21] and integration [22-24]. Many of these functions of NC are a result of its so called general nucleic acid (NA) chaperone activity [21; 25-27]. This property of HIV NC relies on its ability to bind to a diverse array of NA sequences with comparable affinity [27-33], allowing it to chaperone a wide variety of NA annealing and remodeling reactions leading to structures with maximal stability.

In vitro studies have shown that optimal NA chaperone activity requires saturated protein binding corresponding to 1 NC molecule per 6±1 nucleotides (nt) [29; 30; 32-36]. Upon saturation with NC, NA secondary structures are moderately destabilized [37-46]. Wild-type (WT) HIV-1 NC also possesses potent NA aggregating activity [25; 27; 47-49]. Whereas the duplex destabilizing activity of NC has been mapped to its zinc finger domains [39; 50-53], the ability to aggregate NA is largely due to NC's highly cationic N-terminal domain [33; 41; 48; 49; 54]. Recently, the fast kinetics of NC dissociation from both single-stranded (ss) and double-stranded (ds) NA was shown to be another key characteristic of HIV-1 NC's chaperone activity [54; 55].

The effect of NC on the kinetics of annealing complementary NA [18; 27; 29; 34; 36; 50; 56-58] and on various steps of reverse transcription [21; 50; 59-64] has been extensively studied *in vitro*. In all these studies, although stimulation by NC was detected, the magnitude of this effect varied. For example, in studies focusing on annealing of complementary oligonucleotides, the overall rate enhancement measured in the presence of WT HIV-1 NC ranged from 10- to 10^5-fold [18; 29; 34; 36; 58]. One explanation of the variable effect of NC is the wide variety of substrates used in these studies. In a systematic study of NC's chaperone function, the rate of annealing of complementary NA of lower initial stability was shown to be stimulated much less by NC than for substrates with high initial stability [65]. In addition, if the starting structures are too stable, NC's relatively moderate destabilizing activity is unable to facilitate duplex unwinding and annealing [18; 37; 38; 66]. A major factor in NC's ability to stimulate the annealing of highly structured substrates has been attributed to its ability to aggregate NA molecules upon saturated binding [18; 58]. In contrast, sub-saturating levels of NC are sufficient for NA destabilization activity, but generally lead to much weaker stimulation of annealing [37; 38; 40; 58]. These results are consistent with studies using [NC(12-55)], which lacks the cationic N-terminal “aggregation domain” [44; 52; 67]. In general, this truncated NC variant only stimulates annealing by ~10- to 100-fold.

NC has also been demonstrated to stimulate *in vitro* strand transfer reactions that mimic both the annealing and subsequent reverse transcriptase (RT) extension steps. These more complex reactions are monitored by observing the RT extension products on a gel. Interestingly, the effects of NC on stimulation of the complete strand transfer reaction is generally much less (~2- to 3-fold) than the effect observed in simple annealing assays [50; 63; 64; 68-70]. A common feature of these assays is the presence of 6-10 mM Mg^{2+} used in order to optimize RT activity.

A recent study has shown that much lower Mg^{2+} is sufficient to support RT activity [71], and is more relevant to *in vivo* conditions in most cell types. We hypothesize that the presence of high Mg^{2+} concentrations in these strand transfer reactions leads to sub-saturating levels of NC binding, thereby leading to minimal effects of NC on the overall strand transfer process. This hypothesis is qualitatively supported by the recent observation that higher Mg^{2+} suppresses the effect of NC on *in vitro* strand transfer reactions [70].

In this work, we test this hypothesis by performing a systematic study of the effect of Na^{+} and Mg^{2+} ions on NC-stimulated annealing of complementary RNA and DNA hairpins derived from the *trans*-activation response (TAR) element of the HIV genome. Gel-shift assays were used to monitor the kinetics of hairpin annealing over a broad range of NC concentrations, including conditions resulting in NA aggregation. A simple sedimentation assay was used to monitor fractional NA aggregation induced by NC. Taken together, these data help to explain the variable effects of NC's chaperone activity in stimulation of Mg^{2+}-dependent strand transfer reactions, and emphasize the importance of NA saturation with NC for optimal chaperone function *in vitro*.

Results and Discussion

The TAR RNA and DNA substrates used in this work are shown in Figure 1. Both full-length and truncated mini-TAR substrates (Fig 1, boxed) were studied. The two-step annealing process can be described by the following reaction:

$$R+D \underset{k_{-1}}{\overset{k_1 D}{\rightleftarrows}} \mathrm{RD}^{*} \underset{k_{-2}}{\overset{k_2}{\rightleftarrows}} \mathrm{RD} \tag{1}$$

The first bimolecular step leads to the formation of *RD**, characterized by the forward association rate constant k_1, and the intermediate dissociation rate k_{-1}. *RD** is subsequently converted into the fully annealed RNA/DNA duplex, *RD*, via the second monomolecular step, which is characterized by the strand exchange rate k_2 and reverse rate k_{-2}.

Under the majority of solution conditions studied in this work, the TAR RNA/DNA annealing kinetics is bi-exponential. The percent of molecules annealed as a function of time, *P(t)*, can be described as:

$$P(t)=P_{\infty} \cdot (f \cdot (1 - e^{-k_f t})+(1 - f) \cdot (1 - e^{-k_s t})). \tag{2}$$

Here the fast and the slow rates of annealing, k_f and k_s, correspond to the rate of formation of *RD** and *RD*, respectively, while *f* is the probability of intermediate formation and P_{∞} is the final equilibrium percent of RNA annealed. The following equations describe the relationship between these kinetic parameters (eq. (2)) and the elementary rates of the two-step process (eq. (1)) [72]:

$$k_f=k_1 D+k_{-1} \text{ and } k_s=f \cdot k_2+k_{-2}, \tag{3}$$

where

$$f=\frac{k_1 D}{k_1 D+k_{-1}}=\frac{D/K_d^*}{D/K_d^*+1} \text{ and } P_\infty=100\cdot f\cdot\frac{k_2}{k_2+k_{-2}}=100\cdot\frac{D/K_d}{D/K_d+1} \quad (4)$$

Here, K_d* and K_d are the equilibrium dissociation constants of *RD** and *RD*, respectively. Experimentally, both fast and slow rates are observed when they are sufficiently different from each other, i.e. $k_f \gg k_s$, and when the partially annealed complex has an intermediate stability, i.e. $0.1 < f < 0.9$. If *RD** is very stable or very unstable, then only the fast or the slow rate can be determined, respectively. According to eqs. (3) and (4), the fitted parameters k_f, k_s, and f can be used to estimate the elementary rates of the two-step annealing process as:

$$k_1=k_f\cdot\frac{f}{D}, k_{-1}=k_f\cdot(1-f), k_2=k_s/f, K_d^*=\frac{k_{-1}}{k_1}=\frac{(1-f)}{f}\cdot D \quad (5)$$

Hairpin annealing kinetics in the absence of NC

To understand the effects of monovalent and divalent cations on the nucleic acid chaperone activity of HIV-1 NC, we first examined the annealing kinetics of mini-TAR and full-length TAR hairpins (Figure 1) as a function of Na^+ and Mg^{2+} concentration in the absence of NC. As shown in Figure 2 (a and b), Na^+ ions facilitate hairpin annealing, with annealing of the shorter hairpins (Figure 2, panels (a) and (c)) stimulated at much lower salt than the longer TAR substrates (Figure 2, panels (b) and (d)). Mg^{2+} also facilitates hairpin annealing, however, ~10 to 100-fold lower Mg^{2+} is sufficient to achieve the same effect as with Na^+ (Figure 2 (c and d)).

Dependence of intermediate association rate on Na^+ and Mg^{2+}—To quantitatively determine the effect of cations on the annealing kinetics, we fit the annealing time courses in Figure 2 to expression (2) with P_∞=100% (i.e., the annealing of either mini-TAR or TAR is irreversible in the absence of NC) to obtain k_s, k_f and f. The dissociation constant of the intermediate and the elementary reaction rates of the two-step annealing reaction were obtained using eqs. (5), and plotted in Figure 3 as a function of Na^+ and Mg^{2+} concentration. As shown in Figure 3(a), the bimolecular association rate, k_1, is ~10-fold faster for the shorter hairpins with both Na^+ and Mg^{2+}. The fact that this difference between mini and full-length TAR hairpins does not disappear in higher salt suggests that the difference is not due to the stronger electrostatic repulsion between the longer molecules. Shubsda *et al.* also observed slower association of longer hairpins, and attributed this difference to the larger entropy loss upon complex formation [73].

Upon increasing $[Na^+]$ from 20 to 1000 mM or $[Mg^{2+}]$ from 0.2 to 150 mM, k_1 increases from 10^3 to 10^4 $M^{-1}\cdot s^{-1}$ for mini-TAR and from 10^2 to 10^3 $M^{-1}\cdot s^{-1}$ for full-length TAR hairpins. A further increase in the salt concentration does not lead to faster annealing. Consistent with these observations, the rates measured here are significantly slower than the typical association rates of unstructured complementary nucleic acid molecules, which are typically 10^5-10^6 $M^{-1}\cdot s^{-1}$ under similar salt conditions [72; 74-76]. As shown previously, k_1 is stimulated by temperature for mini-TAR [58], suggesting that k_1 involves melting some part of the initial hairpin secondary structure to provide enough base pairing interactions to nucleate stable intermediate formation. Mutational analysis of mini-TAR [58] and full-length TAR RNA/DNA [77] shows that in the absence of NC, annealing proceeds through the formation of an extended loop-loop intermediate (see Figure 1, lower left).

As shown in Figure 3(a) the salt dependence of k_1 is similar for mini-TAR and TAR hairpins. In general, the salt dependence of the rate or equilibrium constant of a process may be characterized by the following equation [78]:

$$s = \frac{d\log k}{d\log M} \tag{6}$$

Here, k is the rate, M is the cation concentration, and s corresponds to the number of cations associating (if s > 0) or dissociating (if s < 0) from the system during the process. For the association process characterized by rate k_1, the values of s were calculated from the slope of a plot of k_1 *vs* $[Na^+]$ or $[Mg^{2+}]$ for both TAR hairpins. For mini-TAR, $s = 0.4 \pm 0.1$ (Na^+) and $s = 0.6 \pm 0.1$ (Mg^{2+}), whereas for full-length TAR, $s = 0.6 \pm 0.1$ (Na^+) and $s = 0.5 \pm 0.1$ (Mg^{2+}). These values are similar to the expected $[Na^+]$ dependence for association rates of short complementary oligonucleotides [75]. These results are also consistent with a single molecule FRET study, wherein a similar s value was measured by studying the $[Mg^{2+}]$-dependence of the docking rate of the hairpin ribozyme [79].

Dependence of intermediate dissociation rate on Na^+ and Mg^{2+}—The dissociation rate, k_{-1}, of the extended 17-bp kissing complex (Figure 1, left) is similar for the mini-TAR and full-length TAR hairpins, and is only weakly dependent on Na^+ and Mg^{2+} concentration (Figure 3(c)). This result is consistent with the formation of a similar intermediate for both short and long DNA/RNA hairpins. Indeed, the average value of $k_{-1} \sim 0.03\ min^{-1}$ is consistent with the expected dissociation rate of a 17-bp duplex at 37 °C [72] and with the fact that in a transition state for nucleic acid strand dissociation, the two strands are still close together with most of the cations still associated [80].

Dependence of the intermediate dissociation constant on Na^+ and Mg^{2+}—The extended kissing complex dissociation constant, K_d*, decreases (i.e., the complex stability increases) with increasing Na^+ or Mg^{2+} concentration (Figure 3(b)). The stabilizing effects of Na^+ and Mg^{2+} are comparable, however, ~100- to 1000-fold higher $[Na^+]$ are required relative to $[Mg^{2+}]$. The bimolecular complex stability (and the annealing kinetics in general (see Figure 2, panels (c) and (d)) saturates at $[Mg^{2+}] \geq 3$ mM for the mini-TAR hairpins and at $[Mg^{2+}] \geq 100$ mM for the full-length TAR hairpins. For both the short and long hairpins, ≥ 1000 mM Na^+ is required to achieved maximal stability. The stability of the extended kissing complex between the shorter mini-TAR hairpins is ~10- to 50-fold higher than that of the longer full-length TAR hairpins under all salt concentrations.

Both monovalent and divalent cations are likely to stabilize the reaction intermediate by facilitating its association rate [72; 75; 81]. Based on the $[Na^+]$ dependence, an s value of -0.3 ± 0.06 was calculated for both the mini-TAR or full-length TAR complexes, further supporting the similar nature of the annealing intermediates. The K_d*-dependence on Mg^{2+} is stronger than for Na^+, with $s = -0.8 \pm 0.1$ for both the mini-TAR and full-length TAR hairpins (see Figure 3(b)). This suggests that up to one additional Mg^{2+} associates with the extended kissing complexes upon intermediate formation. It is possible that this effect is associated with stronger stabilization of inter-helical stacking by Mg^{2+}, as observed in the crystal structure of a hairpin kissing complex [82]. Between two and three Mg^{2+} cations were also shown to associate with the stacked kissing complex of hairpin constructs based on the RNA I/RNA II system [83; 84]. We hypothesize that the relatively strong Mg^{2+} dependence of complex stability is associated with specific Mg^{2+} binding, since non-specific binding is expected to have a very weak ($s \sim -0.1$) Mg^{2+} dependence [80; 81; 85; 86]. Similar results were reported for stabilization of the kissing complex formed by HIV-1 dimerization initiation signal (DIS) hairpins in the presence

of either ~1 mM Mg^{2+} or ~2 M Na^{+}[87]. However, in contrast to our results and in agreement with data for polymeric DNA [72; 88], a stronger dependence of kissing complex stability on Na^{+} than Mg^{2+} was observed [87]. The latter may be related to efficient co-axial stacking of the two hairpin duplexes in the kissing complex, making it more similar to polymeric DNA.

The observed 10- to 50-fold higher stability of the intermediate complex formed by the shorter hairpins appears to be non-electrostatic in origin, since it does not disappear at higher salt. This stability difference is almost entirely due to a faster association rate for the shorter hairpins because the dissociation rate is < 2-fold slower than for full-length TAR (see Figure 3(c)). Therefore, the higher stability of the mini-TAR complex is likely due to a lower cost associated with the reduction in conformational freedom upon kissing complex formation [89].

Dependence of the strand exchange rate on Na^{+} and Mg^{2+}—Figure 3(d) shows the Na^{+} and Mg^{2+} dependence on the strand-exchange rate, k_2. Although slightly more pronounced than for k_{-1}, the salt dependence of k_2 is still very weak, and the rate is reduced in high salt with $s = -0.25 \pm 0.1$. The average value of k_2 over the salt range studied for both TAR systems is ~0.01 min^{-1}, which is about 3-fold slower than k_{-1}. This suggests that the first step of the formation of RD^{*} is in pre-equilibrium to the subsequent strand-exchange step. Surprisingly, the strand-exchange rate for the longer hairpins is practically indistinguishable within experimental accuracy from that of the shorter hairpins. This result suggests that the strand exchange is rate-limited not by opening of the base pairs along the hairpin stem, but by a conformational change, most likely involving cooperative melting of a large fragment of one or both hairpin stems. This hypothesis is in agreement with the fact that the strand exchange rate for four-way junction migration is much faster than the k_2 measured here [90-93].

NC effect on the kinetics of mini-TAR and full-length TAR DNA/RNA annealing

Effect of NC concentration on mini-TAR and full-length TAR RNA/DNA annealing in low salt—Presented in Figure 4 are typical annealing time courses for mini-TAR (a) and full-length TAR (b) hairpins in 20 mM NaCl. Under these low salt conditions, all NC added is expected to be bound to NA. These time courses were fit to equation (2) to obtain k_f, k_s and f, as well as the elementary rates according to eqs. (5). The reaction rates, k_1, k_{-1} and k_2, as well as K_d^{*}, are presented in Figure 6 as a function of fractional saturation of NA with NC, Θ_{NC} (see below). While the two-step mechanism of annealing persists as the NA become saturated with NC, the annealing pathway changes, as described previously for both mini-TAR and TAR [58; 77].

The annealing kinetics was also examined under varying NC/Mg^{2+} solution conditions. Presented in Figure 5 are the annealing time courses of mini-TAR and full-length TAR hairpins measured with two different titration procedures. In the top two panels (mini-TAR (a) and TAR (b)), Mg^{2+} concentration was held constant at 1 mM and NC was varied from 2 to 20 μM. As expected, in both cases the annealing of the hairpins was more effectively facilitated by higher NC concentration. The bottom two panels (mini-TAR (c) and TAR (d)) present the results of a study wherein NC concentration was held constant at 5 μM and Mg^{2+} was varied from 0.5 to 5 mM. Increasing Mg^{2+} slows down the annealing kinetics, with a more dramatic effect on the TAR hairpins. We hypothesize that Mg^{2+} competes with NC for binding to the NA substrates, thereby decreasing the catalytic effect of NC on hairpin annealing. Thus, the dissociation constant of NC, K_d^{NC} (Mg), increases with increasing [Mg^{2+}] and the concentrations of NC that result in similar fractional NC binding, $\Theta_{NC} \sim [NC]/K_d^{NC}([Mg])$, should lead to the same reaction kinetics. In the absence of Mg^{2+}, under the low salt conditions used here, Θ_{NC} is determined simply by the amount of added NC:

$$\Theta_{NC}=(\mathrm{NC:nt}) \times 6 \quad (7)$$

Here, saturated binding (i.e., Θ_{NC} =1) was assumed to be achieved at a value of 1 NC per 6 ± 1 nt [29; 33-36; 94].

Comparison of NC's effect on the elementary rates of hairpin annealing with and without Mg^{2+}—In Figure 6 the elementary reaction rates (k_1, k_{-1}, k_2) and K_d* for mini-TAR and TAR are presented as a function of Θ_{NC}. The reaction rates were determined based on the data shown in Figures 4 and 5. For experiments performed under low salt solution ([Mg^{2+}] =0.2 mM, [Na]=20 mM), Θ_{NC} was determined according to eq. (7). For Mg^{2+}/NC competition assays, Θ_{NC} was estimated for each set of NC and Mg^{2+} concentrations assuming non-specific electrostatic binding of NC and Mg^{2+} (see equations (A1)-(A2) in Supplementary Material). The data from three independent series of experiments are plotted in the graphs shown in Figure 6. A similar dependence of all rates on Θ_{NC} is observed, supporting the hypothesis that nonspecific electrostatic NC/Mg^{2+} competition controls NC's binding and annealing kinetics.

Effect of NC on intermediate association rate—The effect of NC on k_1 is very strong (Figure 6(a)). In all three sets of experiments, the major change in k_1 occurs within the range of $0.2 < \Theta_{NC} < 0.5$ and $0.5 < \Theta_{NC} < 1$ for mini-TAR and TAR RNA/DNA, respectively. In addition, the effect of NC saturation on k_1 for the longer TAR hairpins is significantly greater than for the shorter mini-TAR hairpins. In particular, k_1 for the mini-TAR hairpins increases from ~10^2 $M^{-1}{\cdot}s^{-1}$ in the absence of NC to ~10^5 $M^{-1}{\cdot}s^{-1}$ at saturated NC, while this variation of k_1 is between ~10 $M^{-1}{\cdot}s^{-1}$ and ~4×10^5 $M^{-1}{\cdot}s^{-1}$ for the TAR hairpins. While ~1 M Na^+ or ~10 mM Mg^{2+} is required for maximal k_1 facilitation in the absence of NC (Figure 3 (a)), only ~1 μM NC is sufficient in the absence of Mg^{2+}. In the case of Mg^{2+} or Na^+, k_1 facilitation is a result of better screening of NA charge by these cations. However, k_1 also involves pre-melting of the upper stem of the hairpins, which is probably slightly inhibited by Mg^{2+} and Na^+. As a result, these cations only facilitate k_1 by a factor of ~10 (Figure 3(a)).

In contrast, saturating NC induces ~10^2 and ~10^3 –fold enhancement of k_1 for mini-TAR and TAR, respectively (Figure 6(a)). This effect is most likely the result of two NC properties. First, while Mg^{2+} and Na^+ are only capable of screening NA-NA repulsion, NC additionally induces NA-NA attraction (i.e. aggregation), thereby efficiently facilitating the diffusional search for the complementary sequences. Second, while Mg^{2+} and Na^+ stabilize NA duplexes, thereby slowing down melting of parts of hairpin structures that are in pre-equilibrium to intermediate complex formation, NC destabilizes NA duplexes, thus facilitating intermediate formation.

An approximately 10-fold slower association rate of the longer TAR hairpins relative to the mini-TAR hairpins was observed at $\Theta_{NC} \leq 0.5$. This difference may be attributed to a larger entropy loss upon intermediate complex formation between longer hairpins under non-aggregating solution conditions. However, at Θ_{NC} ~0.8, k_1 for TAR becomes larger and saturates at a value of $\Theta_{NC} \sim 1$, which is ~5-fold higher than for mini-TAR (Figure 6(a)). This difference is most likely due to more facile pre-melting of the critical region involved in intermediate complex nucleation in TAR compared to mini-TAR hairpins and is consistent with the conclusion that mini-TAR and full-length TAR hairpins anneal via different pathways when saturated with NC[77].

Effect of NC on the intermediate dissociation rate—Interestingly, k_{-1} is much less sensitive to variations in Θ_{NC} than k_1 (Figure 6(c)). Moreover, the k_{-1} values for mini-TAR and full-length TAR are almost indistinguishable within the accuracy of the measurements.

The average k_{-1} value over all measurements in the presence of NC ($k_{-1} = 0.12 \pm 0.05$ min^{-1}) is 3-fold higher than the value determined in the absence of NC ($k_{-1} = 0.04 \pm 0.01$ min^{-1}) (compare Figures 3(c) and 6(c)). The k_{-1} values obtained from assays performed in the absence of Mg^{2+} (Figure 6(c), circles) are slightly higher than values measured with Mg^{2+} (Figure 6 (c), squares) but do not show significant variation with Θ_{NC}. In contrast, the k_{-1} values obtained from assays performed with TAR in the presence of 1 mM Mg^{2+} (Figure 6(c), squares) increase by ~4-fold over the range of Θ_{NC} values examined, while assays performed at 5 μM NC and titrated with up to 100 mM Mg^{2+} (Figure 6(c), triangles) increase ~5-fold. This is consistent with the observation that higher Mg^{2+} results in slower duplex dissociation (see Figure 3(c)). The facilitating effect of NC on k_{-1}, expected based on NC's duplex destabilizing ability [18; 58], may be obscured by a change in the annealing pathway from a kissing loop intermediate to a zipper intermediate at high NC [58; 77].

NC's effect on the intermediate dissociation constant—The Θ_{NC} -dependence on K_d* (Figure 6(b)) displays the opposite trend of k_1 (Figure 6(a) and 6(b)). K_d* values vary between ~3×10^{-6} M and 2×10^{-8} M for the mini-TAR hairpins, while the variation for the full-length hairpin is much larger, i.e., between ~10^{-4} M and ~3×10^{-9} M. As observed in the absence of NC, at low Θ_{NC} the K_d* values measured for TAR hairpins are ~10-fold higher than for mini-TAR. However, at $\Theta_{NC} \geq 0.8$, the stability of the TAR intermediate equals that of the mini-TAR hairpins, and at saturating NC, the stability of the TAR intermediate exceeds that of the mini-TAR hairpins (see Figure 6(b)). This likely reflects the fact that full-length TAR and mini-TAR hairpins anneal via different pathways at saturating NC [58; 77].

NC's effect on the strand exchange rate—The k_2 values display the largest scatter and show only a weak growth trend with increasing NC saturation, Θ_{NC} (Figure 6(d)). The k_2 values at low NC saturation vary between the assays, and decrease with Mg^{2+}, in accord with the data presented in Figure 3(d).

Importantly, the k_2 values for mini-TAR and full-length TAR RNA/DNA annealing are similar, just as in the absence of NC. Also, the fact that the strand exchange rate does not depend on the stem length, suggests that the rate-limiting step of strand exchange involves a conformational change preceding bp zippering through the stem. On average, the measured k_2 value is ~2- to 3-fold lower than k_{-1}. This result is in accord with the fact that formation of the reaction intermediate is in pre-equilibrium to strand exchange at all NC concentrations. The average k_2 in the presence of NC (0.03 ± 0.01 min^{-1}) is ~3-fold faster than in the absence of NC (compare Figure 3(d) and 6(d)).

Mini-TAR and TAR aggregation by NC—NC induces nucleic acid aggregation, and NA saturation with NC is required for maximal aggregation activity [18; 27; 29; 34; 47-49; 58]. The latter is a major component of the nucleic acid chaperone activity of NC [58; 77; 95], and facilitates efficient reverse transcription of long DNA products *in vitro* [96; 97].

To quantitatively test the hypothesis that NC-induced NA self-attraction is correlated with Θ_{NC}, and to determine the strength of this attraction, we systematically studied the dependence of fractional NA aggregation, f_a, on Θ_{NC} for mini-TAR and TAR. The conditions of the sedimentation assay were chosen to closely mimic our standard annealing assays. Presented in Figure 7(a) are the results of an NC titration in the presence of 20 mM NaCl and no Mg^{2+}. The fraction of RNA aggregated, f_a, is plotted as a function of Θ_{NC} determined according to eq. (7). Interestingly, the aggregated fraction of NA approximately equals the fractional NC binding (compare the symbols (data points) and the line in Figure 7(a)), i.e., $f_a \approx \Theta_{NC}$. These data are consistent with a 1:6 NC:nt binding at saturation, since aggregation is essentially complete, i.e., $f_a \approx 1$ at $\Theta_{NC} \geq 1$ (Figure 7(a)). It is important to note that the straight line is meant to be a guide to the eye, rather than a strict relationship. Although the sedimentation

assay used here is not as accurate in quantifying the low fractional aggregation regime, the hint of the steeper dependence of f_a on Θ_{NC} can be noticed around $\Theta_{NC} \sim 0.6$, in agreement with the notion that a critical amount of NC saturation is required for aggregation. Mini-TAR and TAR hairpins display similar aggregation behavior (Figure 7 (a) and (b)). However, a shorter 15-nt oligonucleotide under the same solution conditions remained un-aggregated at all concentrations of NC tested (data not shown), in accord with the expectation that the specific level of NA saturation with NC leading to aggregation depends on the oligonucleotide length and concentration. The electrostatic mechanism of multivalent cation-induced NA aggregation leading to such behavior is discussed in the Supplementary Material. This aggregation mechanism also suggests different saturation requirements for aggregation with cationic proteins possessing different charge distributions.

Mini-TAR and TAR aggregation in mixed NC/Mg^{2+} solutions—The fractional NA aggregation was also monitored as a function of Θ_{NC} under conditions of mixed NC/Mg^{2+}/Na^+. In one experiment, Mg^{2+} concentration was fixed at 5 mM and NC was titrated in the range of 1-30 μM. In another set of experiments, NC was fixed at 5 μM and either Mg^{2+}(in the range of 0.5-10 mM) or Na^+ (in the range of 100 to 1000 mM) was varied. As discussed in more detail in the Supplementary Material, this data suggests that the non-electrostatic component of binding free energy of NC to NA is ~ -5 kcal/mol.

Mini-TAR and full-length TAR aggregation data are plotted as f_a vs Θ_{NC} for all of the experiments performed either with or without Mg^{2+} or Na^+ (Figure 7(b)). All f_a (Θ_{NC}) dependencies follow approximately the relationship $f_a \approx \Theta_{NC}$. This result suggests that the fractional RNA aggregation in all of these assays is an approximate measure of the fractional NC binding. Also, these data support the conclusion that the electrostatic competition between NC and Mg^{2+} or Na^+ cations according to equations (A2)-(A3) indeed governs both NC binding and NC-induced NA aggregation.

Conclusions

We previously showed that in the absence of NC, the mini-TAR [58] and full-length TAR [77] hairpins anneal via an extended kissing loop intermediate that involves 17 intermolecular base pairs (see Figure 1, lower left). Here, we demonstrate that k_1 is significantly facilitated by either Na^+ or Mg^{2+} cations, although ~100-fold higher Na^+ is required to produce the same effect. Saturated NC binding enhances k_1 by 100-fold for mini-TAR and by 10^4-fold for full-length TAR hairpins, far exceeding the maximal effect of Na^+ and Mg^{2+} cations (Figure 6(a)). We show that this NC effect on k_1 is related to its ability to aggregate nucleic acids (Figure 7). In addition, in contrast to Na^+ and Mg^{2+} cations, which reduce k_{-1} and k_2 rates by a few fold (Figure 3 (c) and (d)), NC moderately facilitates these rates due to its ability to destabilize NA duplexes [32; 37; 38; 40; 41; 44; 46; 53; 55]. However, the full effect of NC on k_2 in our study is partially masked by the fact that increasing NC also leads to a switch in the annealing pathway from kissing to zipper nucleation[77].

We also show that the effect of Na^+ and Mg^{2+} cations on the chaperone activity of NC is a result of non-specific electrostatic competition for binding to NA. The kinetics is similar under solution conditions that lead to equivalent levels of NC binding to NA (Figure 6). NC behaves effectively as a trivalent cation, with an additional non-electrostatic binding free energy of ~5 kcal/mol of protein, as is discussed in the Supplementary Material [99-101]. This result provides additional support for the hypothesis that NC promotes NA aggregation via a similar electrostatic mechanism as other multivalent cations [102].

Since NA aggregation [47-49] is a sequence non-specific property of NC, we expect these conclusions to hold for the majority of NA sequences. This is consistent with NC's role in

facilitating multiple random strand transfer events during reverse transcription *in vivo*[26; 60; 62; 103; 104]. It is also in agreement with the observation that formation of long reverse transcription products *in vitro* is facilitated under conditions of NC-induced RNA aggregation [96;97]. Based on the estimated NC concentration within the capsid core (~10 mM), NC and viral RNA are expected to be in an aggregated state and it is likely that at least the early stages of reverse transcription occur within this closely packed nucleoprotein complex. It remains an open question whether *in vivo* reverse transcription happens entirely within the RNA/NC aggregate. The traditional view is that the mature HIV-1 capsid disintegrates, i.e., uncoats, prior to the beginning of reverse transcription[103]. However, uncoating is expected to dissolve the RNA/NC aggregate since the equilibrium solution conditions within the cytoplasm correspond to relatively high Mg^{2+} (i.e., low mM) compared to low NC concentration (i.e., < nM). Under these conditions, strand transfer events would not be strongly promoted. On the other hand, if the capsid remains largely intact during reverse transcription and permeable to small ions and nucleotides, but not to the proteins (NC, RT, IN, etc), then the mM concentration of NC present is expected to promote reverse transcription under aggregating conditions. The latter scenario is favored by a recent report showing that the decrease in capsid stability induced either by capsid protein mutations [105; 106] or by the restriction factor Trim5α [107-109], leads to a strong inhibition of reverse transcription. Therefore, the solution conditions that promote the formation of RNA/NC aggregates studied in this work may be relevant for *in vivo* reverse transcription.

Materials and Methods

Protein and nucleic acid preparation

The NC protein used in this work was prepared by solid-phase synthesis as previously described [110], and its purity was estimated to be >95% by SDS-polyacrylamide gel electrophoresis. The concentration of NC was determined by measuring its absorbance at 280 nm and using ε_{280} = 6050 mol^{-1} cm^{-1}.

All DNA oligonucleotides were purchased from Integrated DNA Technologies (Coralville, IA). Mini-TAR RNA (27 nt) was obtained from Dharmacon RNA Technologies (Lafayette, CO). Full-length TAR RNA (59 nt) was generated by *in vitro* transcription.

The concentrations of the RNA and DNA oligonucleotides were determined by measuring their absorbances at 260 nm. The following extinction coefficients were used: mini-TAR RNA (27-mer), 2.82×10^5 M^{-1} cm^{-1}; mini-TAR DNA (32-mer), 3.06×10^5 M^{-1} cm^{-1}; TAR RNA (59-mer), 5.34×10^5 M^{-1} cm^{-1}; TAR DNA (59-mer), 5.65×10^5 M^{-1} cm^{-1}.

Prior to use, all oligonucleotides were refolded in 25 mM Hepes, pH 7.5 and 100 mM NaCl at a concentration 100× that used in the annealing reactions. This was accomplished by incubation at 80 °C for two min and cooling to 60 °C for two min followed by addition of $MgCl_2$ to a final concentration of 10 mM and placement on ice.

Annealing assays

For annealing assays, refolded ^{32}P-labeled RNA (mini-TAR RNA or full-length TAR RNA) was combined with unlabeled complementary DNA in a solution containing 20 mM HEPES (pH 7.5), 20 mM NaCl and 0.2 mM $MgCl_2$, at 37 °C, except when otherwise indicated.

In the absence of NC, studies of the Na^+ and Mg^{2+}-dependence of annealing were performed with 15 nM RNA and 500 nM complementary DNA in the presence of various concentrations of NaCl or $MgCl_2$, as indicated in the figure legends. Reactions were initiated by adding DNA to RNA, followed by incubation in the reaction buffer for the indicated time. Reactions were quenched by placing solutions on ice followed by addition of glycerol to 5% final volume.

Samples were analyzed on 15% or 12% SDS polyacrylamide gels for mini-TAR and full-length TAR annealing, respectively.

Studies of the NC concentration-dependence of annealing were performed by mixing 15 nM RNA and 150 nM complementary DNA. Reactions were initiated by adding NC to final concentrations indicated in the figure legends, followed by incubation in the reaction buffer for the indicated time. In these experiments, the only Mg^{2+} in the final reaction buffer was the amount present due to the RNA and DNA refolding procedure described above (~0.2 mM final). Studies of the Mg^{2+}-dependence of annealing in the presence of NC were performed by incubating 15 nM RNA with 90 nM DNA in the presence of various [Mg^{2+}], as indicated in the figure legends, prior to the addition of 5 μM NC. Annealing reactions were quenched at the indicated times by incubation with 1% (w/v) SDS on ice for 5 min. Samples were subjected to phenol/chloroform-extraction (2×), followed by addition of glycerol to 5% final volume and analyzed on SDS-polyacrylamide gels as described above. All gels were visualized using a Bio-Rad Molecular Imager FX and quantified with Bio-Rad Quantity One Software.

The NC concentration-dependence of annealing in the presence of 1 mM Mg^{2+} was carried out with 15 nM RNA and 90 nM DNA in the presence of four different concentrations of NC (2 μM, 5 μM, 10 μM and 20 μM). All of these NC concentrations correspond to nt:NC ratio <1, i.e. to the large excess of NC, required for NC/NA binding due to high [Mg^{2+}]. The annealing reactions were performed and analyzed as described above.

Sedimentation/aggregation assays

Refolded ^{32}P-labeled mini-TAR or full-length TAR RNA (15 nM) was combined with complementary DNA oligonucleotides (100 nM mini-TAR DNA or 45 nM full-length TAR DNA) in a solution containing 20 mM Hepes (pH 7.5), 20 mM NaCl and 0.2 mM $MgCl_2$. NC was added to final concentrations of 0.1, 0.2, 0.5, 1.0, or 2.0 μM, and reactions (40 μL) were incubated at 37 °C for 30 min. For NC/Mg^{2+} or NC/Na^+ competition assays, 0-20 mM Mg^{2+} or 0-1000 mM Na^+ were titrated in the presence of 5.0 μM NC. Assays were also performed in the presence of a fixed concentration of 5 mM Mg^{2+} and varying concentrations of NC (0 to 30 uM). At the end of the incubation period, solutions were centrifuged at 12,000 rpm in a microcentrifuge for 20 min. Supernatant (5 μL) was collected and analyzed by scintillation counting. The fraction of radioactivity remaining in the supernatant relative to the RNA-only sample (set to 1) was plotted as a function of fractional NC binding, Θ_{NC}.

Supplementary Material

Refer to Web version on PubMed Central for supplementary material.

Acknowledgements

We would like to thank Drs. Daniel G. Mullen and Brandie Kovaleski (University of Minnesota) for chemical synthesis of NC. This research was supported by NIH grant GM065056 (K.M.-F.) and by NIH predoctoral training grant T32 GM008700 awarded to M.-N.V.

References

1. Henderson LE, Bowers MA, Sowder RC 2nd, Serabyn SA, Johnson DG, Bess JW Jr, Arthur LO, Bryant DK, Fenselau C. Gag proteins of the highly replicative MN strain of human immunodeficiency virus type 1: posttranslational modifications, proteolytic processings, and complete amino acid sequences. J Virol 1992;66:1856–65. [PubMed: 1548743]
2. Tritch RJ, Cheng YE, Yin FH, Erickson-Viitanen S. Mutagenesis of protease cleavage sites in the human immunodeficiency virus type 1 gag polyprotein. J Virol 1991;65:922–30. [PubMed: 1987379]

3. Veronese FD, Rahman R, Copeland TD, Oroszlan S, Gallo RC, Sarngadharan MG. Immunological and chemical analysis of P6, the carboxyl-terminal fragment of HIV P15. AIDS Res Hum Retroviruses 1987;3:253–64. [PubMed: 3481270]
4. Dupraz P, Oertle S, Meric C, Damay P, Spahr PF. Point mutations in the proximal Cys-His box of Rous sarcoma virus nucleocapsid protein. J Virol 1990;64:4978–87. [PubMed: 2168981]
5. Rein A. Retroviral RNA packaging: a review. Arch Virol Suppl 1994;9:513–22. [PubMed: 8032280]
6. Hibbert CS, Mirro J, Rein A. mRNA molecules containing murine leukemia virus packaging signals are encapsidated as dimers. J Virol 2004;78:10927–38. [PubMed: 15452213]
7. Muriaux D, Mirro J, Nagashima K, Harvin D, Rein A. Murine leukemia virus nucleocapsid mutant particles lacking viral RNA encapsidate ribosomes. J Virol 2002;76:11405–13. [PubMed: 12388701]
8. Rulli SJ Jr, Hibbert CS, Mirro J, Pederson T, Biswal S, Rein A. Selective and Non-Selective Packaging of Cellular RNAs in Retrovirus Particles. J Virol 2007;81:6623–6631. [PubMed: 17392359]
9. Ako-Adjei D, Johnson MC, Vogt VM. The retroviral capsid domain dictates virion size, morphology, and coassembly of gag into virus-like particles. J Virol 2005;79:13463–72. [PubMed: 16227267]
10. Briggs JA, Johnson MC, Simon MN, Fuller SD, Vogt VM. Cryo-electron microscopy reveals conserved and divergent features of gag packing in immature particles of Rous sarcoma virus and human immunodeficiency virus. J Mol Biol 2006;355:157–68. [PubMed: 16289202]
11. Briggs JA, Simon MN, Gross I, Krausslich HG, Fuller SD, Vogt VM, Johnson MC. The stoichiometry of Gag protein in HIV-1. Nat Struct Mol Biol 2004;11:672–5. [PubMed: 15208690]
12. Muriaux D, Mirro J, Harvin D, Rein A. RNA is a structural element in retrovirus particles. Proc Natl Acad Sci U S A 2001;98:5246–51. [PubMed: 11320254]
13. Prats AC, Housset V, de Billy G, Cornille F, Prats H, Roques B, Darlix JL. Viral RNA annealing activities of the nucleocapsid protein of Moloney murine leukemia virus are zinc independent. Nucleic Acids Res 1991;19:3533–41. [PubMed: 1906602]
14. Weiss S, Konig B, Morikawa Y, Jones I. Recombinant HIV-1 nucleocapsid protein p15 produced as a fusion protein with glutathione S-transferase in Escherichia coli mediates dimerization and enhances reverse transcription of retroviral RNA. Gene 1992;121:203–12. [PubMed: 1280240]
15. Baba S, Takahashi K, Koyanagi Y, Yamamoto N, Takaku H, Gorelick RJ, Kawai G. Role of the zinc fingers of HIV-1 nucleocapsid protein in maturation of genomic RNA. J Biochem (Tokyo) 2003;134:637–9. [PubMed: 14688228]
16. Feng YX, Copeland TD, Henderson LE, Gorelick RJ, Bosche WJ, Levin JG, Rein A. HIV-1 nucleocapsid protein induces “maturation” of dimeric retroviral RNA in vitro. Proc Natl Acad Sci U S A 1996;93:7577–81. [PubMed: 8755517]
17. Barat C, Lullien V, Schatz O, Keith G, Nugeyre MT, Gruninger-Leitch F, Barre-Sinoussi F, LeGrice SF, Darlix JL. HIV-1 reverse transcriptase specifically interacts with the anticodon domain of its cognate primer tRNA. EMBO J 1989;8:3279–85. [PubMed: 2479543]
18. Hargittai MR, Gorelick RJ, Rouzina I, Musier-Forsyth K. Mechanistic insights into the kinetics of HIV-1 nucleocapsid protein-facilitated tRNA annealing to the primer binding site. J Mol Biol 2004;337:951–68. [PubMed: 15033363]
19. Khan R, Giedroc DP. Recombinant human immunodeficiency virus type 1 nucleocapsid (NCp7) protein unwinds tRNA. J Biol Chem 1992;267:6689–95. [PubMed: 1551877]
20. Tisne C, Roques BP, Dardel F. The annealing mechanism of HIV-1 reverse transcription primer onto the viral genome. J Biol Chem 2004;279:3588–95. [PubMed: 14602716]
21. Levin JG, Guo J, Rouzina I, Musier-Forsyth K. Nucleic acid chaperone activity of HIV-1 nucleocapsid protein: critical role in reverse transcription and molecular mechanism. Prog Nucleic Acid Res Mol Biol 2005;80:217–86. [PubMed: 16164976]
22. Thomas JA, Gagliardi TD, Alvord WG, Lubomirski M, Bosche WJ, Gorelick RJ. Human immunodeficiency virus type 1 nucleocapsid zinc-finger mutations cause defects in reverse transcription and integration. Virology 2006;353:41–51. [PubMed: 16784767]
23. Thomas JA, Gorelick RJ. Nucleocapsid protein function in early infection processes. Virus Res 2008;134:39–63. [PubMed: 18279991]
24. Thomas JA, Shulenin S, Coren LV, Bosche WJ, Gagliardi TD, Gorelick RJ, Oroszlan S. Characterization of human immunodeficiency virus type 1 (HIV-1) containing mutations in the

nucleocapsid protein at a putative HIV-1 protease cleavage site. Virology 2006;354:261–70. [PubMed: 16904152]

25. Darlix JL, Lapadat-Tapolsky M, de Rocquigny H, Roques BP. First glimpses at structure-function relationships of the nucleocapsid protein of retroviruses. J Mol Biol 1995;254:523–37. [PubMed: 7500330]
26. Rein A, Henderson LE, Levin JG. Nucleic-acid-chaperone activity of retroviral nucleocapsid proteins: significance for viral replication. Trends Biochem Sci 1998;23:297–301. [PubMed: 9757830]
27. Tsuchihashi Z, Brown PO. DNA strand exchange and selective DNA annealing promoted by the human immunodeficiency virus type 1 nucleocapsid protein. J Virol 1994;68:5863–70. [PubMed: 8057466]
28. Dey A, York D, Smalls-Mantey A, Summers MF. Composition and sequence-dependent binding of RNA to the nucleocapsid protein of Moloney murine leukemia virus. Biochemistry 2005;44:3735–44. [PubMed: 15751950]
29. Dib-Hajj F, Khan R, Giedroc DP. Retroviral nucleocapsid proteins possess potent nucleic acid strand renaturation activity. Protein Sci 1993;2:231–43. [PubMed: 8443601]
30. Fisher RJ, Rein A, Fivash M, Urbaneja MA, Casas-Finet JR, Medaglia M, Henderson LE. Sequence-specific binding of human immunodeficiency virus type 1 nucleocapsid protein to short oligonucleotides. J Virol 1998;72:1902–9. [PubMed: 9499042]
31. Mély Y, de Rocquigny H, Sorinas-Jimeno M, Keith G, Roques BP, Marquet R, Gerard D. Binding of the HIV-1 nucleocapsid protein to the primer tRNA(3Lys), in vitro, is essentially not specific. J Biol Chem 1995;270:1650–6. [PubMed: 7829498]
32. Urbaneja MA, Wu M, Casas-Finet JR, Karpel RL. HIV-1 nucleocapsid protein as a nucleic acid chaperone: spectroscopic study of its helix-destabilizing properties, structural binding specificity, and annealing activity. J Mol Biol 2002;318:749–64. [PubMed: 12054820]
33. Vuilleumier C, Bombarda E, Morellet N, Gerard D, Roques BP, Mély Y. Nucleic acid sequence discrimination by the HIV-1 nucleocapsid protein NCp7: a fluorescence study. Biochemistry 1999;38:16816–25. [PubMed: 10606514]
34. Khan R, Giedroc DP. Nucleic acid binding properties of recombinant Zn2 HIV-1 nucleocapsid protein are modulated by COOH-terminal processing. J Biol Chem 1994;269:22538–46. [PubMed: 8077202]
35. You JC, McHenry CS. HIV nucleocapsid protein. Expression in Escherichia coli, purification, and characterization. J Biol Chem 1993;268:16519–27. [PubMed: 8344933]
36. You JC, McHenry CS. Human immunodeficiency virus nucleocapsid protein accelerates strand transfer of the terminally redundant sequences involved in reverse transcription. J Biol Chem 1994;269:31491–5. [PubMed: 7989315]
37. Azoulay J, Clamme JP, Darlix JL, Roques BP, Mély Y. Destabilization of the HIV-1 complementary sequence of TAR by the nucleocapsid protein through activation of conformational fluctuations. J Mol Biol 2003;326:691–700. [PubMed: 12581633]
38. Beltz H, Azoulay J, Bernacchi S, Clamme JP, Ficheux D, Roques B, Darlix JL, Mély Y. Impact of the terminal bulges of HIV-1 cTAR DNA on its stability and the destabilizing activity of the nucleocapsid protein NCp7. J Mol Biol 2003;328:95–108. [PubMed: 12684000]
39. Beltz H, Clauss C, Piemont E, Ficheux D, Gorelick RJ, Roques B, Gabus C, Darlix JL, de Rocquigny H, Mély Y. Structural determinants of HIV-1 nucleocapsid protein for cTAR DNA binding and destabilization, and correlation with inhibition of self-primed DNA synthesis. J Mol Biol 2005;348:1113–26. [PubMed: 15854648]
40. Beltz H, Piemont E, Schaub E, Ficheux D, Roques B, Darlix JL, Mély Y. Role of the structure of the top half of HIV-1 cTAR DNA on the nucleic acid destabilizing activity of the nucleocapsid protein NCp7. J Mol Biol 2004;338:711–23. [PubMed: 15099739]
41. Bernacchi S, Stoylov S, Piemont E, Ficheux D, Roques BP, Darlix JL, Mély Y. HIV-1 nucleocapsid protein activates transient melting of least stable parts of the secondary structure of TAR and its complementary sequence. J Mol Biol 2002;317:385–99. [PubMed: 11922672]
42. Egele C, Schaub E, Ramalanjaona N, Piemont E, Ficheux D, Roques B, Darlix JL, Mély Y. HIV-1 nucleocapsid protein binds to the viral DNA initiation sequences and chaperones their kissing interactions. J Mol Biol 2004;342:453–66. [PubMed: 15327946]

43. Hong MK, Harbron EJ, O'Connor DB, Guo J, Barbara PF, Levin JG, Musier-Forsyth K. Nucleic acid conformational changes essential for HIV-1 nucleocapsid protein-mediated inhibition of self-priming in minus-strand transfer. J Mol Biol 2003;325:1–10. [PubMed: 12473448]
44. Kankia BI, Barany G, Musier-Forsyth K. Unfolding of DNA quadruplexes induced by HIV-1 nucleocapsid protein. Nucleic Acids Res 2005;33:4395–403. [PubMed: 16077025]
45. Liu HW, Zeng Y, Landes CF, Kim YJ, Zhu Y, Ma X, Vo MN, Musier-Forsyth K, Barbara PF. Inaugural Article: Insights on the role of nucleic acid/protein interactions in chaperoned nucleic acid rearrangements of HIV-1 reverse transcription. Proc Natl Acad Sci U S A 2007;104:5261–7. [PubMed: 17372205]
46. Williams MC, Rouzina I, Wenner JR, Gorelick RJ, Musier-Forsyth K, Bloomfield VA. Mechanism for nucleic acid chaperone activity of HIV-1 nucleocapsid protein revealed by single molecule stretching. Proc Natl Acad Sci U S A 2001;98:6121–6. [PubMed: 11344257]
47. Krishnamoorthy G, Roques B, Darlix JL, Mély Y. DNA condensation by the nucleocapsid protein of HIV-1: a mechanism ensuring DNA protection. Nucleic Acids Res 2003;31:5425–32. [PubMed: 12954779]
48. Le Cam E, Coulaud D, Delain E, Petitjean P, Roques BP, Gerard D, Stoylova E, Vuilleumier C, Stoylov SP, Mély Y. Properties and growth mechanism of the ordered aggregation of a model RNA by the HIV-1 nucleocapsid protein: an electron microscopy investigation. Biopolymers 1998;45:217–29. [PubMed: 9465785]
49. Stoylov SP, Vuilleumier C, Stoylova E, De Rocquigny H, Roques BP, Gerard D, Mély Y. Ordered aggregation of ribonucleic acids by the human immunodeficiency virus type 1 nucleocapsid protein. Biopolymers 1997;41:301–12. [PubMed: 9057495]
50. Guo J, Wu T, Anderson J, Kane BF, Johnson DG, Gorelick RJ, Henderson LE, Levin JG. Zinc finger structures in the human immunodeficiency virus type 1 nucleocapsid protein facilitate efficient minus- and plus-strand transfer. J Virol 2000;74:8980–8. [PubMed: 10982342]
51. Heath MJ, Derebail SS, Gorelick RJ, DeStefano JJ. Differing roles of the N- and C-terminal zinc fingers in human immunodeficiency virus nucleocapsid protein-enhanced nucleic acid annealing. J Biol Chem 2003;278:30755–63. [PubMed: 12783894]
52. Narayanan N, Gorelick RJ, DeStefano JJ. Structure/function mapping of amino acids in the N-terminal zinc finger of the human immunodeficiency virus type 1 nucleocapsid protein: residues responsible for nucleic acid helix destabilizing activity. Biochemistry 2006;45:12617–28. [PubMed: 17029416]
53. Williams MC, Gorelick RJ, Musier-Forsyth K. Specific zinc-finger architecture required for HIV-1 nucleocapsid protein's nucleic acid chaperone function. Proc Natl Acad Sci U S A 2002;99:8614–9. [PubMed: 12084921]
54. Cruceanu M, Gorelick RJ, Musier-Forsyth K, Rouzina I, Williams MC. Rapid kinetics of protein-nucleic acid interaction is a major component of HIV-1 nucleocapsid protein's nucleic acid chaperone function. J Mol Biol 2006;363:867–77. [PubMed: 16997322]
55. Cruceanu M, Urbaneja MA, Hixson CV, Johnson DG, Datta SA, Fivash MJ, Stephen AG, Fisher RJ, Gorelick RJ, Casas-Finet JR, Rein A, Rouzina I, Williams MC. Nucleic acid binding and chaperone properties of HIV-1 Gag and nucleocapsid proteins. Nucleic Acids Res 2006;34:593–605. [PubMed: 16449201]
56. DeStefano JJ. Human immunodeficiency virus nucleocapsid protein stimulates strand transfer from internal regions of heteropolymeric RNA templates. Arch Virol 1995;140:1775–89. [PubMed: 7503678]
57. Heath MJ, Destefano JJ. A complementary single-stranded docking site is required for enhancement of strand exchange by human immunodeficiency virus nucleocapsid protein on substrates that model viral recombination. Biochemistry 2005;44:3915–25. [PubMed: 15751967]
58. Vo MN, Barany G, Rouzina I, Musier-Forsyth K. Mechanistic studies of mini-TAR RNA/DNA annealing in the absence and presence of HIV-1 nucleocapsid protein. J Mol Biol 2006;363:244–61. [PubMed: 16962137]
59. Baird HA, Galetto R, Gao Y, Simon-Loriere E, Abreha M, Archer J, Fan J, Robertson DL, Arts EJ, Negroni M. Sequence determinants of breakpoint location during HIV-1 intersubtype recombination. Nucleic Acids Res 2006;34:5203–16. [PubMed: 17003055]

60. Galetto R, Negroni M. Mechanistic features of recombination in HIV. AIDS Rev 2005;7:92–102. [PubMed: 16092503]
61. Johnson PE, Turner RB, Wu ZR, Hairston L, Guo J, Levin JG, Summers MF. A mechanism for plus-strand transfer enhancement by the HIV-1 nucleocapsid protein during reverse transcription. Biochemistry 2000;39:9084–91. [PubMed: 10924101]
62. Negroni M, Buc H. Recombination during reverse transcription: an evaluation of the role of the nucleocapsid protein. J Mol Biol 1999;286:15–31. [PubMed: 9931246]
63. Roda RH, Balakrishnan M, Hanson MN, Wohrl BM, Le Grice SF, Roques BP, Gorelick RJ, Bambara RA. Role of the Reverse Transcriptase, Nucleocapsid Protein, and Template Structure in the Two-step Transfer Mechanism in Retroviral Recombination. J Biol Chem 2003;278:31536–46. [PubMed: 12801926]
64. Rodriguez-Rodriguez L, Tsuchihashi Z, Fuentes GM, Bambara RA, Fay PJ. Influence of human immunodeficiency virus nucleocapsid protein on synthesis and strand transfer by the reverse transcriptase in vitro. J Biol Chem 1995;270:15005–11. [PubMed: 7541033]
65. Derebail SS, Heath MJ, DeStefano JJ. Evidence for the differential effects of nucleocapsid protein on strand transfer in various regions of the HIV genome. J Biol Chem 2003;278:15702–12. [PubMed: 12595541]
66. Cosa G, Harbron EJ, Zeng Y, Liu HW, O'Connor DB, Eta-Hosokawa C, Musier-Forsyth K, Barbara PF. Secondary structure and secondary structure dynamics of DNA hairpins complexed with HIV-1 NC protein. Biophys J 2004;87:2759–67. [PubMed: 15454467]
67. Godet J, de Rocquigny H, Raja C, Glasser N, Ficheux D, Darlix JL, Mély Y. During the early phase of HIV-1 DNA synthesis, nucleocapsid protein directs hybridization of the TAR complementary sequences via the ends of their double-stranded stem. J Mol Biol 2006;356:1180–92. [PubMed: 16406407]
68. Guo J, Wu T, Kane BF, Johnson DG, Henderson LE, Gorelick RJ, Levin JG. Subtle alterations of the native zinc finger structures have dramatic effects on the nucleic acid chaperone activity of human immunodeficiency virus type 1 nucleocapsid protein. J Virol 2002;76:4370–8. [PubMed: 11932404]
69. Heilman-Miller SL, Wu T, Levin JG. Alteration of nucleic acid structure and stability modulates the efficiency of minus-strand transfer mediated by the HIV-1 nucleocapsid protein. J Biol Chem 2004;279:44154–65. [PubMed: 15271979]
70. Wu T, Heilman-Miller SL, Levin JG. Effects of nucleic acid local structure and magnesium ions on minus-strand transfer mediated by the nucleic acid chaperone activity of HIV-1 nucleocapsid protein. Nucleic Acids Res 2007;35:3974–87. [PubMed: 17553835]
71. Goldschmidt V, Didierjean J, Ehresmann B, Ehresmann C, Isel C, Marquet R. Mg^{2+} dependency of HIV-1 reverse transcription, inhibition by nucleoside analogues and resistance. Nucleic Acids Res 2006;34:42–52. [PubMed: 16394022]
72. Cantor, CR.; Schimmel, PR. Biophysical Chemistry Part III The Behavior of Biological Macromolecules. W. H. Freeman & Co.; San Francisco: 1980.
73. Shubsda MF, McPike MP, Goodisman J, Dabrowiak JC. Monomer-dimer equilibrium constants of RNA in the dimer initiation site of human immunodeficiency virus type 1. Biochemistry 1999;38:10147–57. [PubMed: 10433723]
74. Bloomfield, VA.; Crothers, DM.; Tinoco, I. Nucleic Acids Structure, Properties, and Function. University Science Books; Sausalito, CA: 2000.
75. Porschke D. The dynamics of nucleic-acid single-strand conformation changes. Oligo- and polyriboadenylic acids. Eur J Biochem 1973;39:117–26. [PubMed: 4770785]
76. Wetmur JG, Davidson N. Kinetics of renaturation of DNA. J Mol Biol 1968;31:349–70. [PubMed: 5637197]
77. Vo MN, Barany G, Rouzina I, Musier-Forsyth K. HIV-1 Nucleocapsid protein switches the pathway of TAR RNA/DNA annealing from loop-loop “kissing” to “zipper”. 2008submitted
78. Lohman TM, DeHaseth PL, Record MT Jr. Analysis of ion concentration effects of the kinetics of protein-nucleic acid interactions. Application to lac repressor-operator interactions. Biophys Chem 1978;8:281–94. [PubMed: 728535]

79. Bokinsky G, Rueda D, Misra VK, Rhodes MM, Gordus A, Babcock HP, Walter NG, Zhuang X. Single-molecule transition-state analysis of RNA folding. Proc Natl Acad Sci U S A 2003;100:9302–7. [PubMed: 12869691]
80. Manning GS. On the application of polyelectrolyte limiting laws to the helix-coil transition of DNA. V. Ionic effects on renaturation kinetics. Biopolymers 1976;15:1333–43. [PubMed: 949538]
81. Williams AP, Longfellow CE, Freier SM, Kierzek R, Turner DH. Laser temperature-jump, spectroscopic, and thermodynamic study of salt effects on duplex formation by dGCATGC. Biochemistry 1989;28:4283–91. [PubMed: 2765487]
82. Jossinet F, Paillart JC, Westhof E, Hermann T, Skripkin E, Lodmell JS, Ehresmann C, Ehresmann B, Marquet R. Dimerization of HIV-1 genomic RNA of subtypes A and B: RNA loop structure and magnesium binding. Rna 1999;5:1222–34. [PubMed: 10496223]
83. Gregorian RS Jr, Crothers DM. Determinants of RNA hairpin loop-loop complex stability. J Mol Biol 1995;248:968–84. [PubMed: 7539081]
84. Marino JP, Gregorian RS Jr, Csankovszki G, Crothers DM. Bent helix formation between RNA hairpins with complementary loops. Science 1995;268:1448–54. [PubMed: 7539549]
85. Blagoi YP, Sorokin VA, Valeyev VA, Khomenko SA, Gladchenko GO. Magnesium ion effect on the helix-coil transition of DNA. Biopolymers 1978;17:1103–18. [PubMed: 656550]
86. Krakauer H. A thermodynamic analysis of the influence of simple mono- and divalent cations on the conformational transitions of polynucleotide complexes. Biochemistry 1974;13:2579–89. [PubMed: 4831904]
87. Weixlbaumer A, Werner A, Flamm C, Westhof E, Schroeder R. Determination of thermodynamic parameters for HIV DIS type loop-loop kissing complexes. Nucleic Acids Res 2004;32:5126–33. [PubMed: 15459283]
88. Frank-Kamenetskii F. Simplification of the empirical relationship between melting temperature of DNA, its GC content and concentration of sodium ions in solution. Biopolymers 1971;10:2623–4. [PubMed: 5126533]
89. Shubsda M, Goodisman J, Dabrowiak JC. Characterization of hairpin-duplex interconversion of DNA using polyacrylamide gel electrophoresis. Biophys Chem 1999;76:95–115. [PubMed: 11396505]
90. Hohng S, Wilson TJ, Tan E, Clegg RM, Lilley DM, Ha T. Conformational flexibility of four-way junctions in RNA. J Mol Biol 2004;336:69–79. [PubMed: 14741204]
91. Joo C, McKinney SA, Lilley DM, Ha T. Exploring rare conformational species and ionic effects in DNA Holliday junctions using single-molecule spectroscopy. J Mol Biol 2004;341:739–51. [PubMed: 15288783]
92. Karymov M, Daniel D, Sankey OF, Lyubchenko YL. Holliday junction dynamics and branch migration: single-molecule analysis. Proc Natl Acad Sci U S A 2005;102:8186–91. [PubMed: 15917329]
93. McKinney SA, Tan E, Wilson TJ, Nahas MK, Declais AC, Clegg RM, Lilley DM, Ha T. Single-molecule studies of DNA and RNA four-way junctions. Biochem Soc Trans 2004;32:41–5. [PubMed: 14748709]
94. Paoletti AC, Shubsda MF, Hudson BS, Borer PN. Affinities of the nucleocapsid protein for variants of SL3 RNA in HIV-1. Biochemistry 2002;41:15423–8. [PubMed: 12484783]
95. Stewart-Maynard KM, Cruceanu M, Wang F, Vo MN, Gorelick RJ, Williams MC, Rouzina I, Musier-Forsyth K. Retroviral NC proteins display non-equivalent levels of nucleic acid chaperone activity. J Virol. 2008in press
96. Anthony RM, Destefano JJ. In vitro synthesis of long DNA products in reactions with HIV-RT and nucleocapsid protein. J Mol Biol 2007;365:310–24. [PubMed: 17070544]
97. Mirambeau G, Lyonnais S, Coulaud D, Hameau L, Lafosse S, Jeusset J, Borde I, Reboud-Ravaux M, Restle T, Gorelick RJ, Le Cam E. HIV-1 protease and reverse transcriptase control the architecture of their nucleocapsid partner. PLoS ONE 2007;2:e669. [PubMed: 17712401]
98. Yuan Y, Kerwood DJ, Paoletti AC, Shubsda MF, Borer PN. Stem of SL1 RNA in HIV-1: structure and nucleocapsid protein binding for a 1 × 3 internal loop. Biochemistry 2003;42:5259–69. [PubMed: 12731867]
99. Nguyen TT, Rouzina I, Shklovskii BI. Reentrant condensation of DNA induced by multivalent counterions. J Chem Phys 2000;112:2562–2568.

100. Rouzina I, Bloomfield VA. Macroion attraction due to electrostatic correlation between screening counterions. 1. Mobile surface-adsorbed ions and diffuse ion cloud. J Phys Chem 1996;100:9977–9989.

101. Zhang R, Shklovskii BI. Phase diagram of aggregation of oppositely charged colloids in salty water. Phys Rev E Stat Nonlin Soft Matter Phys 2004;69:021909. [PubMed: 14995493]

102. Bloomfield VA. DNA condensation by multivalent cations. Biopolymers 1997;44:269–82. [PubMed: 9591479]

103. Coffin, JM.; Hughes, SH.; Varmus, HE. Retroviruses. Cold Spring Harbor Laboratory Press; 1997.

104. Hu WS, Rhodes T, Dang Q, Pathak V. Retroviral recombination: review of genetic analyses. Front Biosci 2003;8:d143–55. [PubMed: 12456341]

105. Forshey BM, von Schwedler U, Sundquist WI, Aiken C. Formation of a human immunodeficiency virus type 1 core of optimal stability is crucial for viral replication. J Virol 2002;76:5667–77. [PubMed: 11991995]

106. Ganser-Pornillos BK, Yeager M, Sundquist WI. The structural biology of HIV assembly. Curr Opin Struct Biol 2008;18:203–17. [PubMed: 18406133]

107. Diaz-Griffero F, Perron M, McGee-Estrada K, Hanna R, Maillard PV, Trono D, Sodroski J. A human TRIM5alpha B30.2/SPRY domain mutant gains the ability to restrict and prematurely uncoat B-tropic murine leukemia virus. Virology 2008;378:233–42. [PubMed: 18586294]

108. Perron MJ, Stremlau M, Lee M, Javanbakht H, Song B, Sodroski J. The human TRIM5alpha restriction factor mediates accelerated uncoating of the N-tropic murine leukemia virus capsid. J Virol 2007;81:2138–48. [PubMed: 17135314]

109. Stremlau M, Perron M, Welikala S, Sodroski J. Species-specific variation in the B30.2(SPRY) domain of TRIM5alpha determines the potency of human immunodeficiency virus restriction. J Virol 2005;79:3139–45. [PubMed: 15709033]

110. Liu HW, Cosa G, Landes CF, Zeng Y, Kovaleski BJ, Mullen DG, Barany G, Musier-Forsyth K, Barbara PF. Single-molecule FRET studies of important intermediates in the nucleocapsid-protein-chaperoned minus-strand transfer step in HIV-1 reverse transcription. Biophys J 2005;89:3470–9. [PubMed: 16100256]

111. Zuker M. Mfold web server for nucleic acid folding and hybridization prediction. Nucleic Acids Res 2003;31:3406–3415. [PubMed: 12824337]

Abbreviations

TAR
: *trans*-activation response element

NC
: nucleocapsid protein

bp
: base pair

NA
: nucleic acid (s)

nt
: nucleotide (s)

ss
: single-stranded

ds
: double-stranded

HIV-1
: human immunodeficiency virus type 1

WT

wild-type

RT

reverse transcriptase

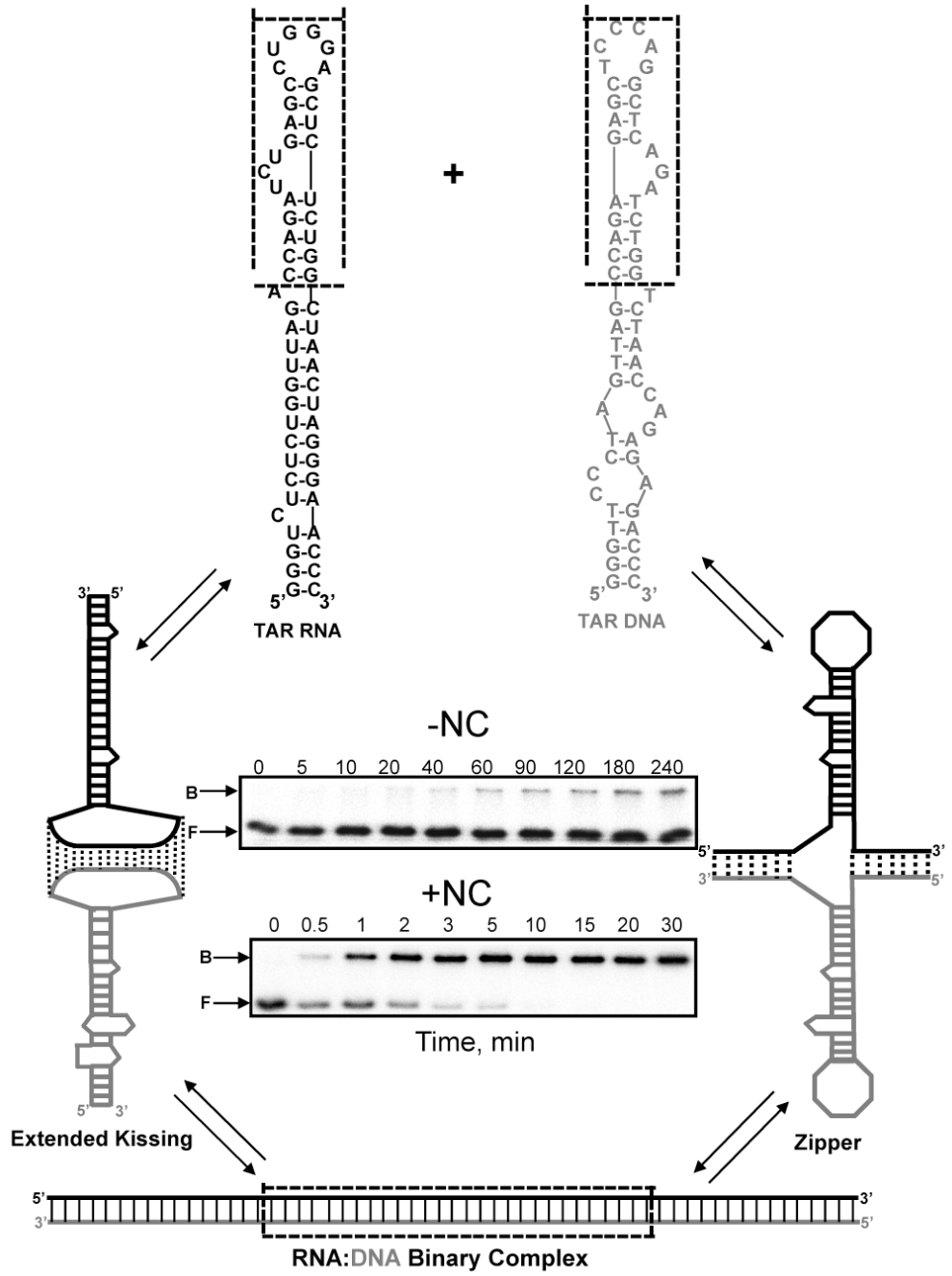

Figure 1.

Multiple pathways of TAR RNA/DNA annealing. Predicted secondary structures of full-length and mini-TAR RNA (black) and DNA (gray) hairpins are shown at the top. Sequences are derived from the HIV-1 NL4-3 isolate, and secondary structures were predicted by *m*-fold analysis [111]. The mini-TAR constructs are derived from the top part of each hairpin (dotted box). In the absence of NC, mini-TAR and full-length TAR RNA/DNA annealing involve initial formation of an extended loop-loop kissing interaction (middle, left) followed by strand exchange to form the fully annealed duplex (bottom). In the presence of saturating amounts of NC, full-length TAR RNA/DNA annealing involves nucleation through the 3′/ 5′ termini resulting in formation of a “zipper” intermediate (middle, right) prior to conversion to the fully

annealed product[58,77]. Typical gels used to measure the TAR RNA/DNA annealing reaction time course in the absence (top) and presence (bottom) of saturating amounts of NC are also shown. The gel lanes are labeled with the reaction time in minutes. The bands corresponding to the bound and the free RNA are labeled B and F, respectively.

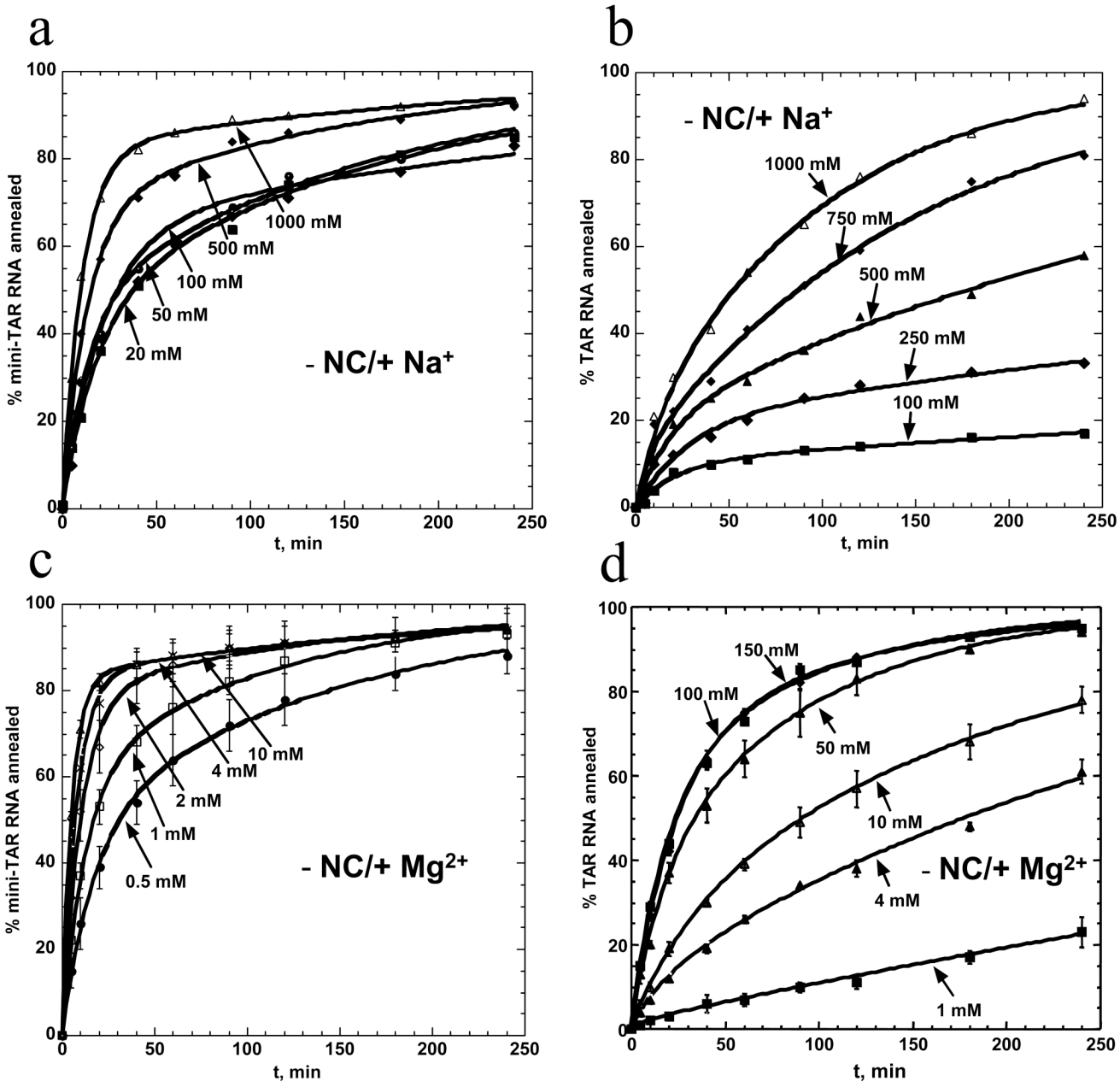

Figure 2.

Na^+ and Mg^{2+} dependence of mini-TAR and full-length TAR RNA RNA/DNA annealing in the absence of NC. Percent mini-TAR (a) and (c) or full-length TAR (b) and (d) RNA (15 nM) annealed to complementary DNA (300 nM) as a function of time at 37 °C in the presence of various concentrations of NaCl and $MgCl_2$, as indicated on each curve. Lines represent two exponential fits of the data to equation (2), with the equilibrium percent annealed fixed at 100%.

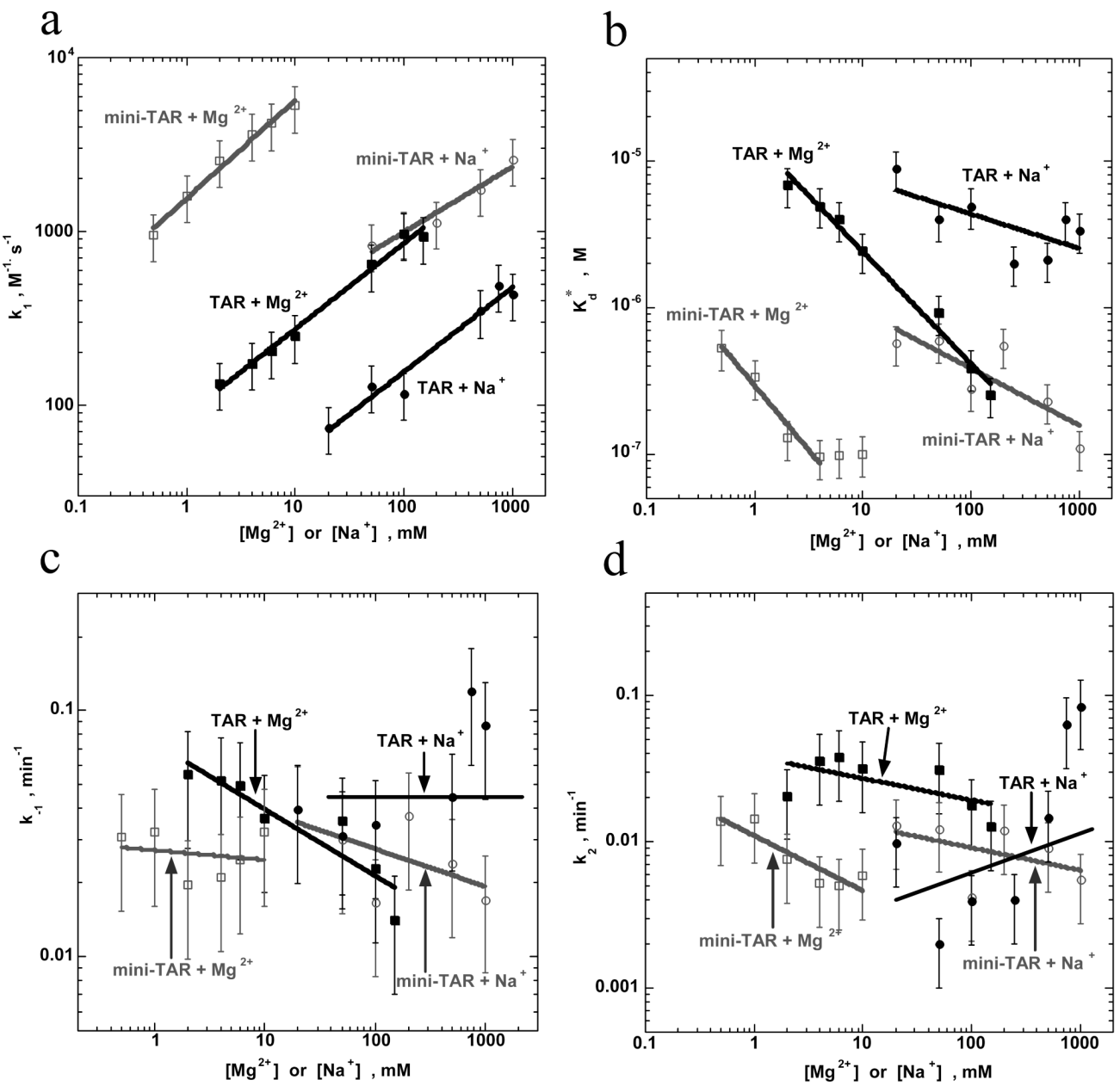

Figure 3.

Dependence of the intermediate dissociation constant and elementary rates of mini-TAR or full-length TAR RNA/DNA annealing on Na^+ and Mg^{2+} in the absence of NC. (a) Intermediate association rate k_1, (b) dissociation constant K_d*, (c) dissociation rate k_{-1}, and (d) strand exchange rate k_2 as a function of Na^+ and Mg^{2+} concentration. The elementary reaction rates are obtained based on the data shown in Figure 2. Gray and black lines represent mini-TAR and full-length TAR RNA/DNA annealing, respectively.

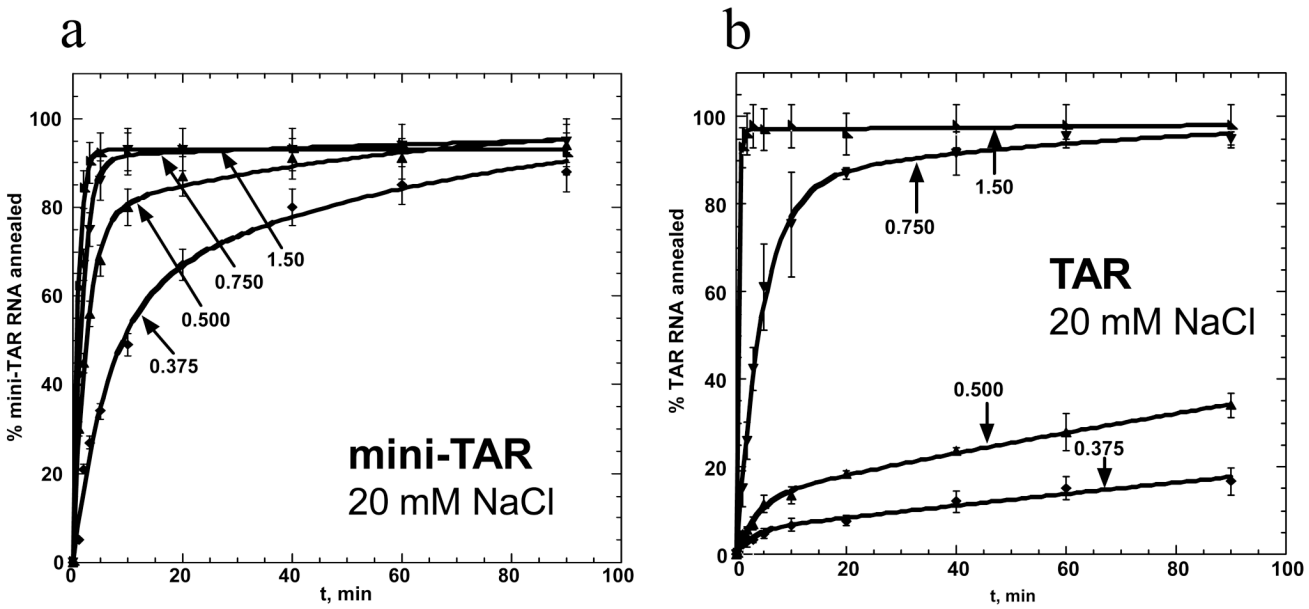

Figure 4.

NC concentration-dependence of mini-TAR and full-length TAR RNA/DNA annealing in low salt. Percent mini-TAR (a) or full-length TAR (b) RNA (15 nM) annealed to 150 nM complementary DNA as a function of time in the presence of various concentrations of NC in 20 mM NaCl and 0.2 mM $MgCl_2$. Numbers indicate the fractional NC binding, Θ_{NC}, as defined according to eq. (2). Lines represent two-exponential fits of the data.

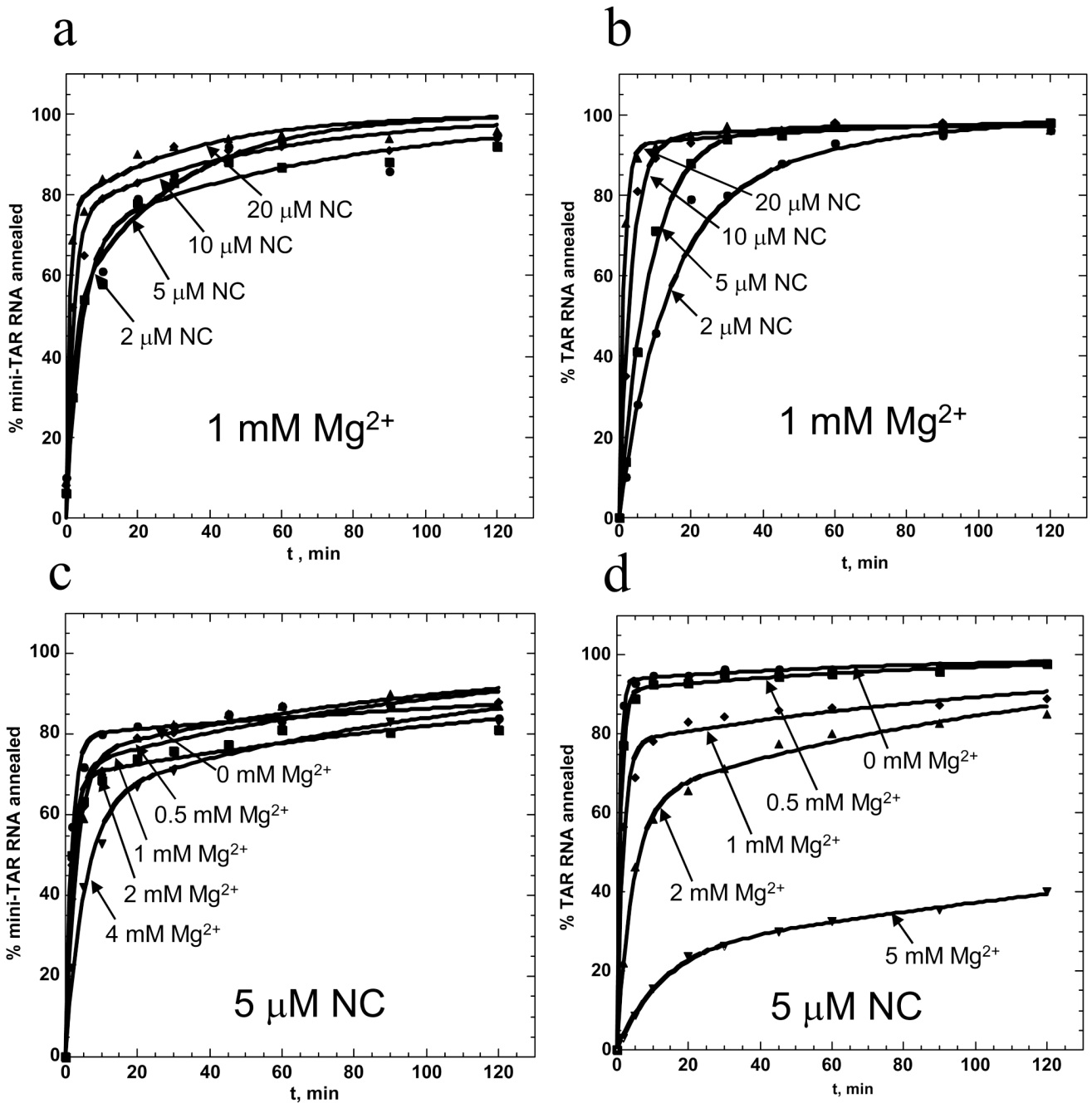

Figure 5.

Mg^{2+} dependence of NC-facilitated mini-TAR and full-length TAR RNA/DNA annealing. Percent mini-TAR (a) or full-length TAR (b) RNA (15 nM) annealed to complementary DNA (90 nM) as a function of time with 1 mM $MgCl_2$ in the presence of various concentrations of NC, as indicated on each curve. Percent mini-TAR (c) or full-length TAR (d) RNA (15 nM) annealed to 90 nM complementary DNA as a function of time with 5 μM NC in the presence of various concentrations of $MgCl_2$, as indicated on curve. Lines represent two-exponential fits of the data.

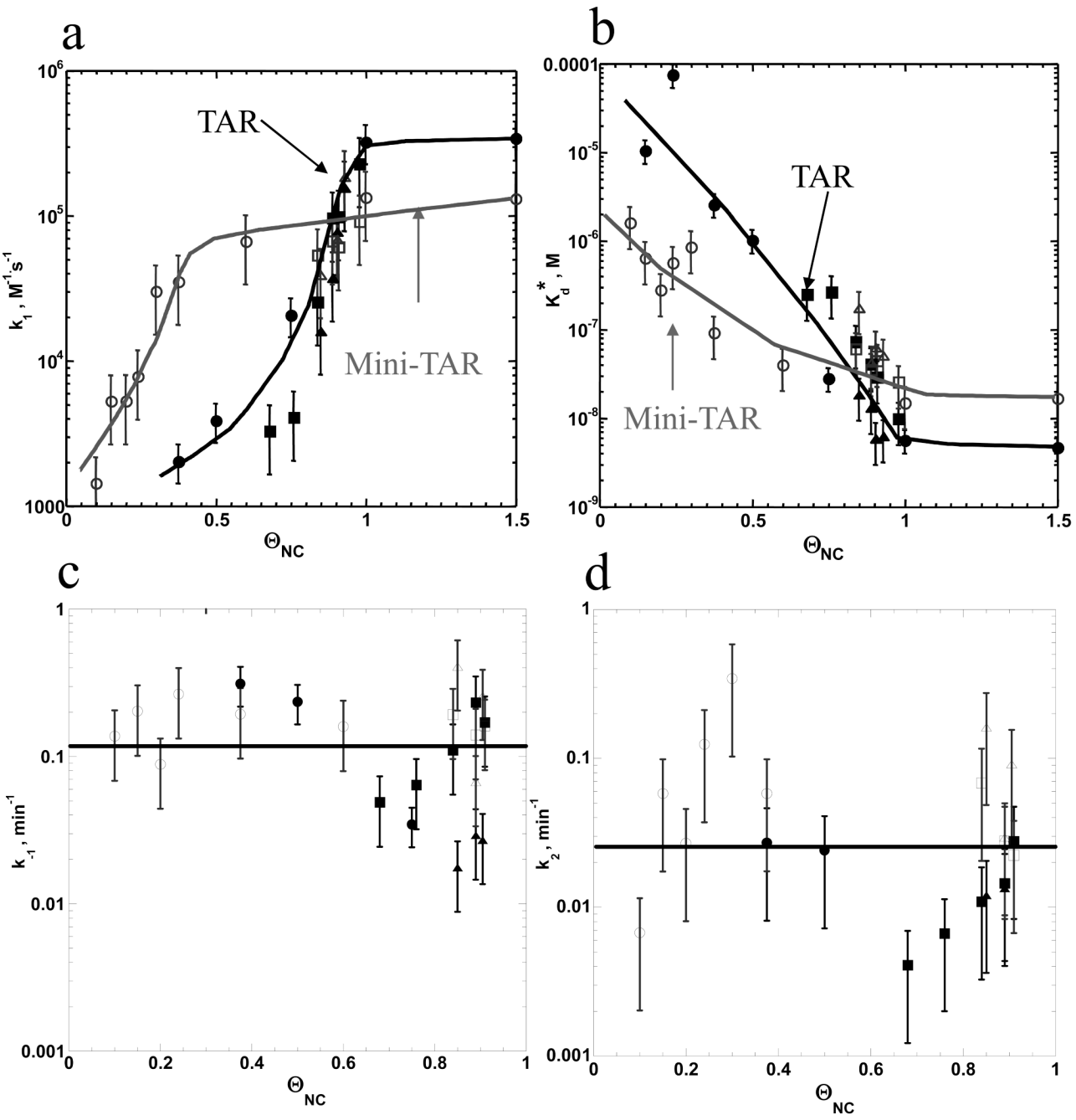

Figure 6.

Elementary rate analyses of mini-TAR (gray lines and symbols) and full-length TAR (black lines and symbols) RNA/DNA annealing as a function of fractional NC binding, Θ_{NC}. The elementary reaction rates, k_1 (a), K_d^* (b), k_{-1} (c) and k_2 (d), were determined using the equations (3) and (4) based on three independent sets of experiments: titration of NC with no $MgCl_2$ (Figure 3), titration of NC with 1 mM $MgCl_2$ (Figure 4(a) and (b)), and titration of $MgCl_2$ with 5 μM NC (Figure 4(c) and (d)). Θ_{NC} was estimated using equation (2) for the assays with no $MgCl_2$. For the assays performed in the presence of Mg^{2+}, Θ_{NC} was estimated for each set of NC and $MgCl_2$ concentrations assuming non-specific electrostatic binding of NC and $MgCl_2$ to nucleic acid using equations (A1)-(A3) in the Supplementary Material. Symbols represent

data obtained from titration of NC with no $MgCl_2$ (circles), with 1 mM $MgCl_2$ (squares) and from titration of $MgCl_2$ with 5 μM NC (triangles). Open symbols represent mini-TAR and fill symbols represent full-length TAR annealing. Lines are guides for the eye.

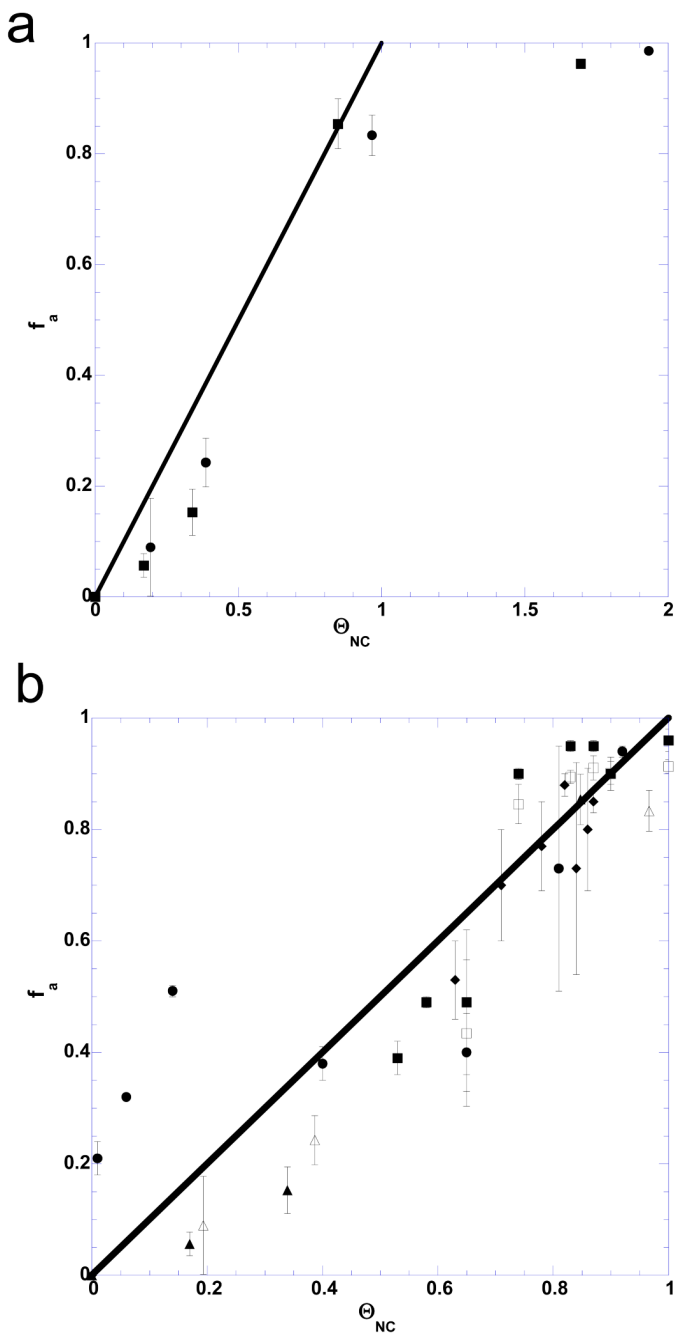

Figure 7.

Dependence of fraction of mini-TAR and full-length TAR RNA aggregated, f_a, on fractional NC binding, Θ_{NC}. (a) Experimental f_a values obtained in sedimentation experiments performed in the absence of Mg^{2+}. Θ_{NC} was calculated according to eq. (7). RNA aggregation for either mini-TAR (circles) or full-length TAR (squares) saturates upon NA saturation with NC, i.e. at $\Theta_{NC} \geq 1$. (b) Plot of the f_a *versus* Θ_{NC} values from panel (a) (triangles), along with the results of additional sedimentation experiments: NC titration in the presence of 5 mM Mg^{2+} (circles), as well as Mg^{2+} (squares) or Na^+ (diamonds) titration in the presence of 5 μM NC. In panel (b), open symbols correspond to mini-TAR and closed symbols correspond to full-length TAR substrates. The straight line in both panels corresponds to $f_a = \Theta_{NC}$.